Studies on the carbon reactions in the anode of deposited carbon fuel cells

X.-Y. Zhao, Q. Yao[*], S.-Q. Li, N.-S. Cai

Key Laboratory for Thermal Science and Power Engineering of Ministry of Education, Department of Thermal Engineering, Tsinghua University, Beijing 100084, China

ARTICLE INFO

ABSTRACT

The carbon reactions in the anode of deposited carbon fuel cells were studied experimentally and theoretically. Deposition experiments were conducted by decomposing methane in a thermogravimetric analyzer at 800 °C, with both NiO or YSZ powders and small chips of an unused anode-supported SOFC button cell used separately as bed materials. The carbon tended to deposit on the Ni surfaces with the NiO or YSZ powders, while with the anode chips, the deposited carbon formed particles comparable in size to the Ni or YSZ particles with little carbon deposited near the electrolyte where the electrochemical reactions occur. Thus, the results infer that the deposited carbon has little opportunity to participate in the electrochemical reactions. A two-dimensional isothermal model was then developed to examine the influence of the deposited carbon on the cell performance. The results show the diffusion coefficient of CO has the largest influence, followed by the gasifying reactivity and the electrochemical reactivity of the carbon. Finally, a short deposition time and a high methane concentration are favored to improve the performance of deposited carbon fuel cells.

© 2008 Elsevier B.V. All rights reserved.

1. Introduction

High temperature fuel cells with carbon fuels (carbon or coal), termed here as direct carbon fuel cells (DCFC), have received more attention in recent years [1,2]. Compared to the traditional hydrogen fuels for fuel cells, carbon fuels are abundant and easily obtained. At the same time, this fuel cell can enhance the utilization efficiency of carbon fuels, which is our key need before renewable energy sources become dominant as energy shortages increase. Since the entropy of carbon's reaction with oxygen is negative, the thermal efficiency ($\eta = \Delta G/\Delta H = 1 - T\,\Delta S/\Delta H$) can reach as high as 100%. In addition, since the carbon and oxidants (air or pure oxygen) are separated, the carbon dioxide in the exhaust gases is concentrated and, thus, can be easily recovered. With solid fuels, DCFCs can have high energy densities and stable operating voltages.

Three kinds of DCFCs have been developed with different electrolytes, i.e., molten carbonate, molten hydroxide and solid oxide [2–4]. DCFCs with molten electrolytes were found to be suitable for large power plants. However, in such systems, the coal must first be decomposed into conductive chars to obtain efficient reactions at the anode. Also the electrolyte can quickly be contaminated by the introduction of impurities from natural carbon resources [3]. DCFCs with molten hydroxide electrolytes have a unique electrolyte con-

sumption problem caused by the CO_2 product. Methods are needed to reduce the electrolyte consumption rate or to recover the electrolyte [4]. DCFCs with solid oxide electrolytes are now becoming a promising alternative, since they do not need complex systems or special treatment of the coal fuel and can be easily made portable.

Solid oxide DCFCs are categorized according to the contact between the carbon fuel with the anode, i.e., systems where the carbon does not contact or only physically contacts the anode and systems where the carbon is chemically bonded to the anode. Nakagawa et al. [5] and Gür and Huggins [6] studied a physical contact system by placing the carbon fuel adjacent to the platinum anode and measuring the voltages and current densities in the fuel cells. Gür and co-workers [2] further demonstrated the feasibility of the concept using commercially available ceramic tubes in a modified SOFC design that utilized He as the fluidization medium. Their experiments produced large anodic polarizations and low power densities (8–20 mW cm^{-2}). In such systems, the carbon in the anode chamber cannot directly react with the oxygen ions because the carbon is not located at the triple phase boundary (TPB), which is the reaction zone of an SOFC [2,7]. To improve the contact with the anode reactive sites and to reduce the large polarizations in solid oxide DCFCs, Ihara et al. [8] deposited pyrolytic carbon from methane decomposition on the anode as the fuel. After the carbon deposition, the experimental system was purged with argon and the power generation experiment was started. Power densities as high as 66.5 (mW cm^{-2}) were obtained with a design for a quickly rechargeable direct carbon solid oxide fuel cell (RDCFC) with propane for recharging [7]. In this system, the carbon

* Corresponding author. Tel.: +86 10 62782108; fax: +86 10 62794068.
E-mail addresses: zhao-xy02@mails.tsinghua.edu.cn (X.-Y. Zhao),
yaoq@tsinghua.edu.cn (Q. Yao).

Nomenclature

c	concentration (mol m^{-3})
D	diffusion coefficient (m^2 s^{-1})
F	Faraday constant (96,485 C mol^{-1})
ΔG	electrochemical reaction activation energy (J mol^{-1})
i	current density (A cm^{-2})
i_0	exchange current density (A cm^{-2})
I	total current (A)
M_i	molecular weight of species i
P	pressure (Pa)
R	gas constant (8.314 J (mol K)$^{-1}$)
S_c	carbon effective reactive areas per unit volume (m^2 m^{-3})
S_{TPB}	TPB active area per unit volume (m^2 m^{-3})
T	temperature (K)
V	voltage (V)
w_i	mass fraction of species i
x_i	mole fraction of species i

Greek letters

α	transfer coefficient
ε	porosity
η	overpotential (V)
ρ	density (kg m^{-3})
σ	conductivity (S m^{-1})
τ	tortuosity

Subscripts

An	anode
Avg	average
Ca	cathode
Elec	electronic
Ion	ionic
Inter	interface

Subscripts

Bulk	bulk phase
Eff	effective
Kn	Knudsen
MS	Maxwell–Stefan
TPB	triple phase boundary

is connected chemically with the anode. However, the anodic reactions in these systems are very complex with not only the carbon's electrochemical reactions on the solid surfaces, but also possible carbon gasification reactions. Secondly, CO also reacts electrochemically at the anode and competes with the carbon reaction at the active sites, which makes the design optimization of the fuel cell more difficult. Thirdly, the carbon structures and the deposition area may change during operation as the anode conditions change with time [8].

For the carbon electrochemical reactions, Ihara et al. [8] proposed that the carbon reacts directly with the chemisorbed oxygen atoms around the TPB lines after the oxygen ions lose two electrons. Therefore, the carbon needs to be located near the TPB lines. Huang and Huang [9] proposed another carbon reaction mechanism after a series of experiments with both Ni/GDC and Ni/YSZ anodes. They observed a fuel-free current during intermittent fuel flow over the Ni/YSZ anode in direct methane SOFCs, with current produced without any fuel existing at the anode. They concluded that the fuel-free current is due to the effect of the electrochemical promotion of bulk lattice-oxygen extraction. For this extraction,

Huang and Huang [10] further proposed when O^{2-} is transported to the anode side where it may donate an electron to the bulk lattice oxygen to form O$^-$, the mobility of the lattice-oxygen species to form additional CO$_x$ products [10] may be increased. This second mechanism enlarges the reaction sites so that the deposited carbon also has a chance to react with oxygen ions on the Ni surface as well as in the vicinity of the TPB [11]. This kind of reaction is due to the mixed ionic–electronic character of the GDC anode material [10]. However, YSZ has a lower electronic conductivity than GDC, so Ni/YSZ anodes are less likely to react in this way. A third solid oxide fuel cell electrochemical reaction mechanism was reported by Horita et al. [12]. They put graphite or coal adjacent to the YSZ electrolyte without any catalyst or electrode material. Small currents were generated in the device with graphite producing a larger current than coal due to better electronic conductivity. Besides these limited studies, these are few other studies on the deposited carbon anode reactions. Although the deposited carbon reactions at the anode are quite important, the role of these reactions on the fuel cell performance has not yet been reported. In addition, the roles of other factors, i.e., the carbon gasification reactions and the interior diffusion, still need to be evaluated to improve fuel cell designs. These needs are the focus of this paper.

This paper first conducts experiments with decomposing methane in a thermogravimetric analyzer (TGA) using both NiO or YSZ powders and small chips of an unused anode-supported SOFC button cell as bed materials to evaluate the role of electrochemical reactions or other factors on cell performance. Then, a two-dimensional isothermal model is developed to quantitatively compare the influences of the electrochemical reactions, carbon gasification reactions and the interior diffusion.

2. Experimental

2.1. Deposition on the surfaces of NiO and YSZ powders

A thermogravimetric analyzer (TGA, TA 2100) was used for all the deposition experiments. The carbon deposition locations, either the Ni or YSZ surfaces, determine the kinds of reactions in the cells. To illustrate these effects, the first series of deposition experiments separately used commercial NiO powder (Inco Ltd., Canada) and 8 mol% yttria-stabilized ZrO$_2$ powder (YSZ, TOSOH, Japan) as the bed catalysts. The experiments started with the pre-reduction of the catalysts at 850 °C by feeding a mixture of H$_2$:Ar (99.999%) = 10:90 to the catalyst bed at a total flow rate of 100 ml min^{-1}. As the reduction was completed, the catalyst bed was purged with pure Argon at 100 ml min^{-1} and the temperature was equilibrated at 800 °C. Then, the carbon was deposited on the catalyst surfaces by feeding a mixture of CH$_4$:Ar = 10:90 at a total flow rate of 100 ml min^{-1} for 15 min. The methane flow was then switched off and the temperature was gradually decreased to room temperature with an argon purge. All the experimental conditions used here were similar to those used in real fuel cells [13].

2.2. Deposition inside chips of an unused anode-supported button cell

A second series of carbon deposition experiments were performed in the same TGA (TA 2100) using small chips of an unused anode-supported button cell as the bed catalyst. The details of the cell preparation were given by [14]. The button cell was used instead of the NiO or YSZ powders because the button cells have very different micro-structures than the naturally mixed NiO–YSZ powders due to sintering, cooling and other treatments. During the experiments, the button cells were broken into pieces and laid in the crucible with the anode surface facing upward. The experi-
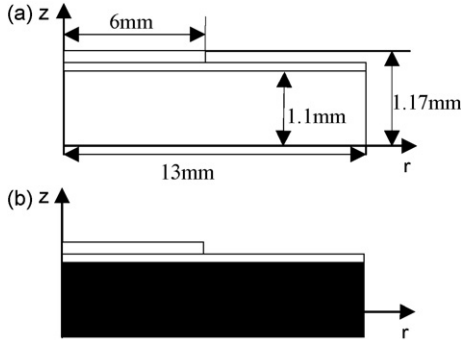
Fig. 1. Two-dimensional axisymetrical model geometry: (a) for the button fuel cell; (b) for the button fuel cell with carbon deposited inside the anode.

mental procedure was the same as in Section 2.1. Four different groups of methane decomposition times and concentrations were used: $CH_4:Ar = 10:90$ fed for 10 min, $CH_4:Ar = 50:50$ fed for 10 min, $CH_4:Ar = 10:90$ fed for 30 min and $CH_4:Ar = 50:50$ fed for 30 min. The total flow rate was kept at 100 ml min^{-1} for all runs. After the methane decomposition, cross-sections of the cell pieces were characterized using a scanning electronic microscope (SEM) with an electron probe microanalyzer (S-4500, Hitachi, Japan) to evaluate the different patterns of the deposited carbon that determine the reaction mechanisms, including carbon particle sizes, particle aggregation and the deposition distribution along the anode thickness. These SEM pictures were then analyzed quantitively by the software ImageJ to compare the porosities and mean pore sizes under different feeding conditions.

3. Analysis

Two models were developed to analyze the deposition process. The first model is an anode-supported button cell model as illustrated in Fig. 1(a) without a carbon layer, fed by a mixture of CO and CO$_2$. After the experimental validation of the first model, a second model was developed to predict the deposition in carbon fuel cells by adding a carbon layer as large as the anode into the first model. Although the deposited carbon fuel cell model is similar to the CO fueled SOFC (the first model), the deposited carbon

changes the anode exchange current, i_{an}, the CO diffusion coefficient in the anode, D_{CO}, and the partial pressures of CO caused by the gasification of the carbon. Thus, i_{an} and D_{CO} in the second model, are changed and a third parameter, k_c, is specially introduced to represent the effect of carbon gasification.

3.1. Model geometry and assumptions

The models assumed the two-dimensional axially symmetric geometry illustrated in Fig. 1. The model assumptions are:

(1) The button cell operates at steady state.
(2) The gas mixtures are considered to be ideal gases.
(3) The active reaction sites are assumed to be uniformly distributed in each layer of electrodes and carbons. The cathode and anode both have two electronic and ionic conducting phases with the two conducting phases assumed to be continuous and homogeneous in both electrodes.
(4) The two models are isothermal.
(5) The thermal convection is neglected in the porous electrode compared to the diffusion through all the layers. Pressure gradients in the porous electrode are also neglected.
(6) The potentials and species concentrations are assumed to be uniform at the electrode/gas and carbon/gas channel interfaces.

The SOFC button fuel cell model and carbon fuel cell models were formulated with these assumptions and model geometries using charge balance and mass balances equations together with the electrochemical reaction kinetics and chemical reaction kinetics (especially for the carbon reactions) as described in the later sections.

3.2. Governing equations

The governing equations for the first model were given by Shi et al. [14]. Several parameters which were changed in this model are:

- CO is assumed take the only reactant on the TPB, so surface diffusion is negligible.
- The anodic exchange current density is selected as 7.3×10^3 A m^{-2} according to previous experimental data [13].
- The open-circuit state is chosen as the reference state with the experimentally measured open-circuit voltage used here for simplicity.
- In the carbon layer, only the reaction $C + CO_2 \rightarrow 2CO$ is taken into account. The kinetic rate constant $k_c = 4.016 \times 10^8 \exp(-29790/T)$ (m s^{-1}) [15] is used in the second model calculation.

The governing equations for the electrode charge balances for both models are summarized in the following equations.

- Ionic and electronic balances at the cathode:

$$-\nabla \cdot (\sigma_{ion,ca} \nabla V_{ion,ca}) = -i_{0,ca} S_{TPB,ca} \left(\frac{c_{O_2}^{TPB}}{c_{O_2}^{Bulk}} \exp \left(\frac{\alpha n_e F(V_{elec,ca} - V_{ion,ca} - V_{ref,ca})}{RT} \right) - \exp \left(-\frac{(1-\alpha) n_e F(V_{elec,ca} - V_{ion,ca} - V_{ref,ca})}{RT} \right) \right) \tag{1}$$

$$-\nabla \cdot (\sigma_{elec,ca} \nabla V_{elec,ca}) = i_{0,ca} S_{TPB,ca} \left(\frac{c_{O_2}^{TPB}}{c_{O_2}^{Bulk}} \exp \left(\frac{\alpha n_e F(V_{elec,ca} - V_{ion,ca} - V_{ref,ca})}{RT} \right) - \exp \left(-\frac{(1-\alpha) n_e F(V_{elec,ca} - V_{ion,ca} - V_{ref,ca})}{RT} \right) \right) \tag{2}$$

- Ionic and electronic balances at the anode:

$$-\nabla \cdot (\sigma_{ion,an} \nabla V_{ion,an}) = i_{0,an} S_{TPB,an} \left(\frac{c_{CO}^{TPB}}{c_{CO}^{Bulk}} \exp \left(\frac{\alpha n_e F(V_{elec,an} - V_{ion,an} - V_{ref,an})}{RT} \right) - \frac{c_{CO_2}^{TPB}}{c_{CO_2}^{Bulk}} \exp \left(-\frac{(1-\alpha) n_e F(V_{elec,an} - V_{ion,an} - V_{ref,an})}{RT} \right) \right) \tag{3}$$

$$-\nabla \cdot (\sigma_{elec,an} \nabla V_{elec,an}) = -i_{0,an} S_{TPB,an} \left(\frac{c_{CO}^{TPB}}{c_{CO}^{Bulk}} \exp \left(\frac{\alpha n_e F(V_{elec,an} - V_{ion,an} - V_{ref,an})}{RT} \right) - \frac{c_{CO_2}^{TPB}}{c_{CO_2}^{Bulk}} \exp \left(-\frac{(1-\alpha) n_e F(V_{elec,an} - V_{ion,an} - V_{ref,an})}{RT} \right) \right) \tag{4}$$

Then, the governing equations for the electrode mass balances for first model in Fig. 1(a) are:
- Mass balance at the anode:

$$-\nabla \cdot (\rho w_{CO} D_{CO,CO_2}^{eff} \nabla x_{CO}) = \frac{-i_{trans,CO} S_{TPB} M_{CO}}{2F} \tag{5}$$

- Mass balance at the cathode:

$$-\nabla \cdot (\rho w_{O_2} D_{O_2,N_2}^{eff} \nabla x_{O_2}) = \frac{-i_{trans,O_2} S_{TPB} M_{O_2}}{4F} \tag{6}$$

The governing equation for the cathode mass balances for second model in Fig. 1(b) is the same with that in Fig. 1(a). However,

	Ionic charge balance	Electronic charge balance	Mass balance
Cathode–air interface	Insulated	$V_{cell,ca}$	$w_{O_2,bulk}, w_{N_2,bulk}$
Electrolyte–air interface	Insulated	Insulated	Insulated
Cathode–electrolyte interface	Continuity	Insulated	Insulated
Anode–electrolyte interface	Continuity	Insulated	Insulated
Anode–fuel interface	Insulated	$V_{cell,an}$	$w_{CO,bulk}, w_{CO_2,bulk}$
Axis	Symmetric	Symmetric	Symmetric
Others	Insulated	Insulated	Insulated

the governing equation for the anode side of the second model in Fig. 1(b) combines the effect of the deposited carbon's gasification,

$$-\nabla \cdot (\rho w_{CO} D^{eff}_{CO,CO_2} \nabla x_{CO}) = \frac{-i_{trans,CO} S_{TPB} M_{CO}}{2F}$$

$$+ 2k_c \times S_c \times x_{CO_2} \times M_{CO} \times \frac{P}{RT} \quad (7)$$

where S_c describes the carbon effective reactive areas per cubic meter carbon, which are dependent on the carbon types and the porosity of carbon packing. S_c was assumed to be of $100\,(m^2\,m^{-3})$ here.

3.3. Boundary conditions

The boundary conditions are specified in Table 1. The difference between $V_{cell,an}$ and $V_{cell,ca}$ is the voltage used in the calculation. Here, $V_{cell,an} = 0$ and $V_{cell,ca}$ was changed to get different current densities. $w_{i,bulk}$ is the mass fraction of species i in the fuel or air channel. For boundary Insulated and Symmetric boundaries, the partial derivative of each variable at the boundary was zero, with flux through the Symmetric boundary.

3.4. Solution method

The model was solved using the finite element commercial software COMSOL MULTIPHSICS®, version 3.1. The current density distributions were calculated for a given voltage. The average current density calculated from the current density distribution is:

$$i_{avg} = \frac{I_{total}}{A} = \frac{1}{R^2} \int_0^R 2r i_{local}\, dr \quad (8)$$

where R is the cathode radius. A specific average current density value was determined for each voltage to plot V–i curve.

4. Results and discussion

4.1. Carbon deposition on Ni and YSZ surfaces

The time-dependent CH_4 dissociation rate on the Ni and YSZ surfaces are illustrated in Fig. 2(a) and (b) for a CH_4:Ar feed composition of 10:90 at a flow rate of $100\,ml\,min^{-1}$. The weight increment of Ni was about 1% over 15 min while that of YSZ was inappreciable for the same time. Similarly, Choudhary et al. [16] reported much larger surface areas of Ni surfaces covered by carbon than YSZ surfaces using an indirect method using X-ray Photoelectron Spectroscopy (XPS) to analyze the Ni and YSZ surface ratios before and after the experiment (including methane decomposition and carbon gasification). Their results support the TGA results in Fig. 2. Therefore, the deposition of carbon in practical cell anodes made of mixed Ni–YSZ powders cannot be uniform. This reduces the probability of carbon atoms contacting the interface between YSZ and Ni
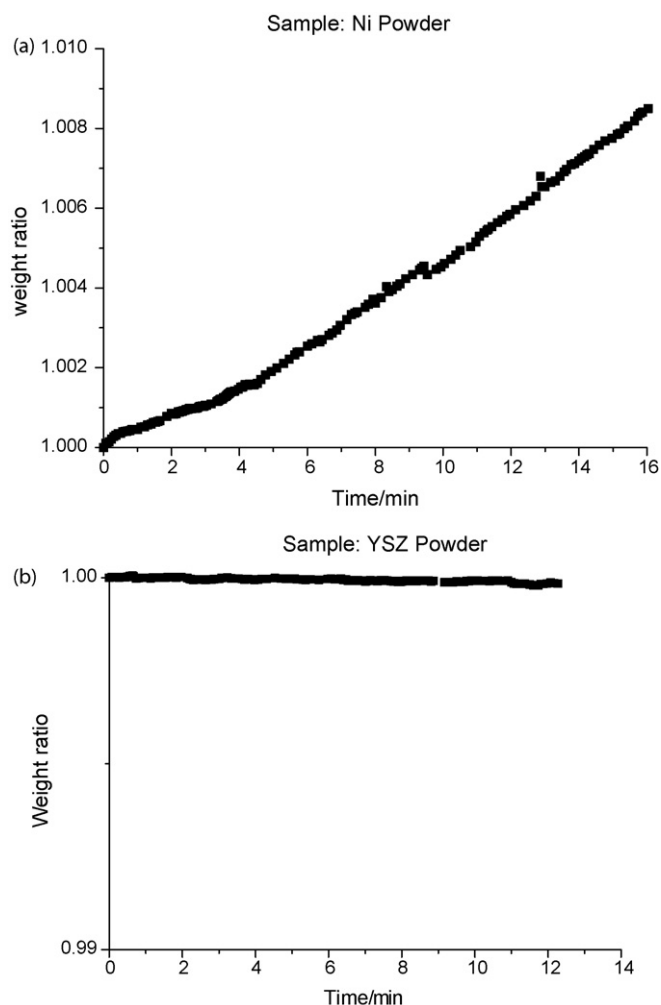

Fig. 2. Sample weight ratio, starting from the methane cracking: (a) Ni (%); (b) YSZ (%).

particles, i.e., the TPB lines, which further reduces the possibility of the carbon's electrochemical reactions.

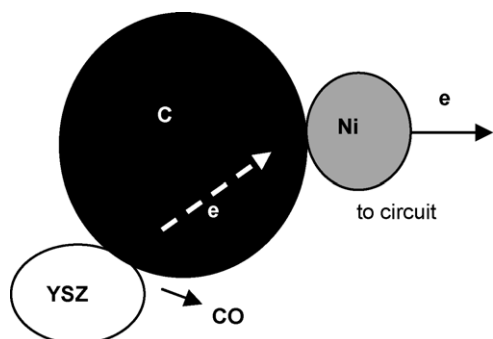### 4.2. Distribution of deposited carbons along the anode

Besides the nonuniformity of the carbon deposition on the Ni and YSZ surfaces of the anode, the carbon was also not deposited uniformly along the thickness direction, as indicated by the SEM images of cross-sections of the cell chips shown in Fig. 3. When a CH_4:Ar mixture of 50:50 at a flow rate of $100\,ml\,min^{-1}$ was fed for 30 min, the deposited carbon particles near the electrolyte shown in Fig. 3(b) were smaller and fewer than near the free surface as shown in Fig. 3(a). Similar results are seen in Fig. 3(c) and (d) for a CH_4:Ar mixture of 10:90 fed at a rate of $100\,ml\,min^{-1}$ for 30 min. A similar phenomenon was also reported by Barnett and co-workers [17] who attributed it to the high concentrations of the products and the low concentration of the reactant near the electrolyte during methane decomposition. Since the region near the electrolyte is the location of the strongest electrochemical reactions [18], the few deposited carbon particles in this location further implies a reduction in the possibility of the carbon's electrochemical reactions.

The nonuniform distributions of the deposited carbon on both the Ni and YSZ surfaces and along the thickness direction indicate that few carbon atoms have a chance to react directly with oxygen ions or chemisorbed oxygen. However, the preference of
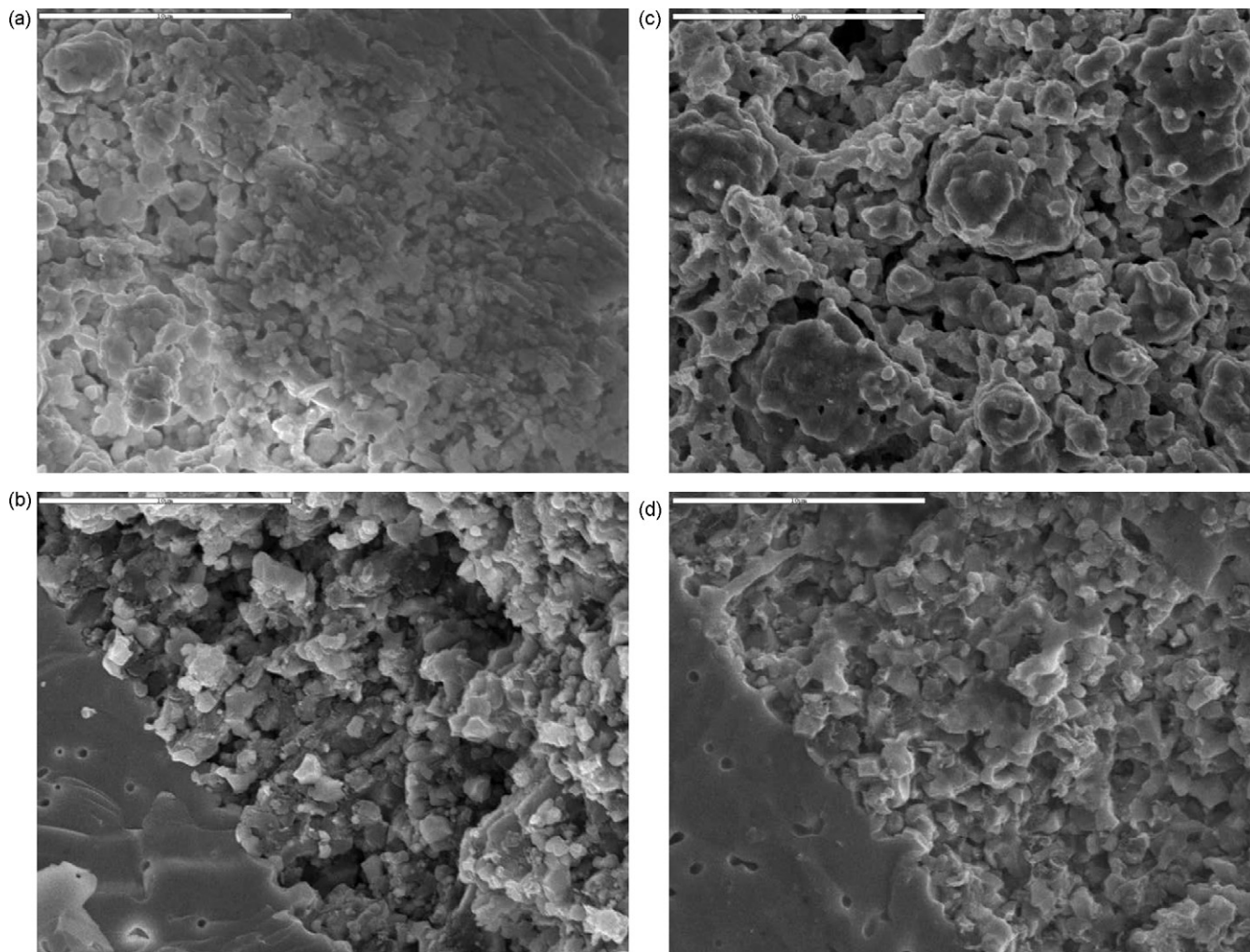
Fig. 3. SEM images of the anode cross-section: (a) edge of the anode (50% CH$_4$, 30 min); (b) near the electrolyte (50% CH$_4$, 30 min); (c) edge of the anode (10% CH$_4$, 30 min); (d) near the electrolyte (10% CH$_4$, 30 min).

carbon deposition on the Ni surfaces may facilitate the reaction mechanism reported by Horita et al. [12]. Since deposited carbon atoms on supported Ni catalysts are graphitic above 873 K [19], the carbon atoms deposited here at 1073 K are surely graphitic and electronic-conductive. Therefore, carbon atoms on the Ni surface need to only contact the YSZ surfaces instead of the TPB lines for the electrochemical reaction, as illustrated in Fig. 4. Although this mechanism can enlarge the possibility of electrochemical reactions of the deposited carbon atoms, this reaction is still too weak to

contribute to the cell performances, because of the low coverage of carbon in these key electrochemical zones and the low reaction rates of carbon reported in Horita's experiments [12].

4.3. Sizes and aggregation of the deposited carbon

The patterns of the deposited carbon inside the anode after the methane decomposition at four different feed conditions are shown in Fig. 5. Increases of the deposition time from 10 to 30 min not only made the carbon structure denser, but also resulted in aggregated 5–10 μm carbon particles with sizes up to 5–10 μm. Thus, the primary deposited carbon structures at 30 min (Fig. 5(b) and (d)) were less uniform than at 10 min (Fig. 5(a) and (c)). Increases of the methane concentration from 10% to 50% only made the deposited carbon slightly denser, without significant changes in the sizes of the primary carbon particles (Fig. 5(a) and (c)).

The porosity and mean pore size analysis results of all the SEM pictures in the experiments by the software ImageJ are shown in Table 2. Compared to the measured values of the same unused fuel cell without deposited carbon, the porosities and mean pore sizes in the four working conditions were all reduced. The porosities of the deposited carbon structures at 30 min were much lower than that at 10 min, while the mean pore sizes at 30 min were slightly lower than that at 10 min. Both porosities and mean pore
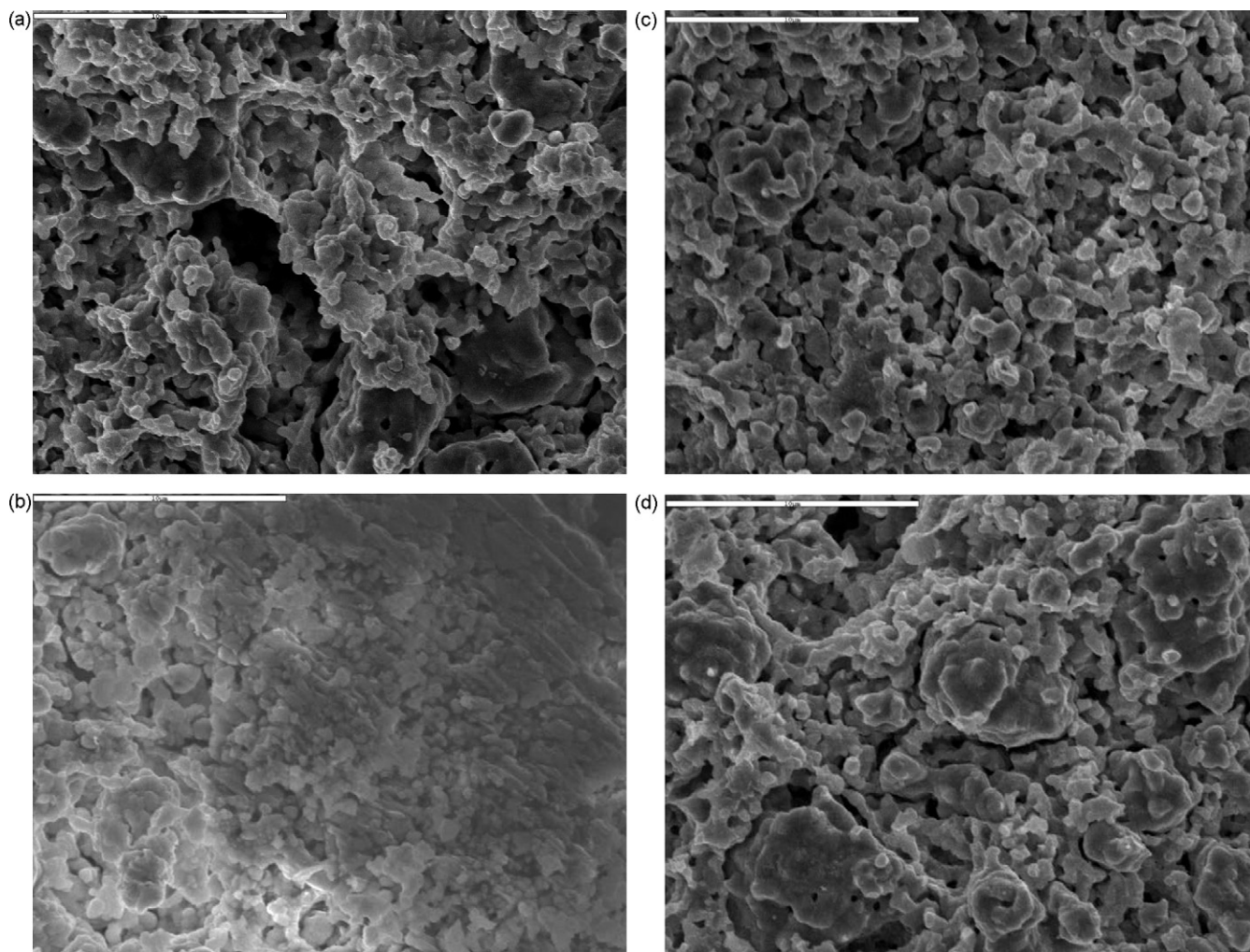

Fig. 4. Illustration of the direct carbon electrochemical oxidization.

Fig. 5. SEM images of the edges of the anode: (a) 50% CH$_4$, 10 min; (b) 50% CH$_4$, 30 min; (c) 10% CH$_4$, 10 min; (d) 10% CH$_4$, 30 min.

sizes were almost the same at different methane concentration but the same deposition times. Thus, longer decomposition times may lead to serious sintering of the carbon structures (Fig. 5(a) and (b)) that greatly deteriorates the diffusion in the anode, while larger methane concentrations do not affect diffusion so much. Thus, high concentrations instead of large deposition times will more effectively increase the carbon deposition rates in the anode and so are suggested for portable use.

Additionally, the sizes of the primary deposited carbon elements in Fig. 5 were comparable to the sizes of the Ni and YSZ particles, which were 1–2 μm. Three different solid particles cannot have the same contact lines, especially three comparably sized solid particles. Thus, very little of the carbon was deposited at the TPB lines.

Therefore, these results suggest that the deposited carbon had little opportunity to reach the TPB lines or the intense electrochemical reaction regions; thus, it had little possibility of reacting electrochemically. Although no fuel presented as the electrochemical reactant at the anode in the beginning of the power generation circle, the fuel cell can still generate electricity by the oxygen con-centration difference between the anode and cathode. The oxygen diffused to the anode will then react with the deposited carbon to make CO or CO$_2$. With the accumulation of CO, the electrochemical reaction of CO will dominate at the anode.

Even so, a comparison of these electrochemical reactions with other factors in the cells such as the carbon gasification reactions and the interior diffusion conditions is essential to understand deposited carbon fuel cells. Since these effects are difficult to compare experimentally, a model was developed to explore the influences of the electrochemical reactions, the carbon gasification reactions and the interior diffusion conditions.

4.4. Model calculation results

The SOFC button fuel cell model is first verified using experimental data for a CO fueled anode-supported button cell [13]. S_{TPB} and D_{CO} were adjusted to fit the experimental data because they could not be obtained directly from the literature. Here, S_{TPB} was set to 4.3×10^3 m^2 m^{-3}, and D_{CO} was set to 6.5×10^{-6} m^2 s^{-1} for the case

Table 2
Porosities and mean pore sizes for various conditions by ImageJ

	50%, 10 min	50%, 30 min	10%, 30 min	10%, 10 min	Without carbon [15]
Porosity	0.1732	0.1259	0.1154	0.1605	0.27
Mean pore sizes (μm)	0.25	0.21	0.19	0.22	0.48

Fig. 6. Model validation results.

Fig. 8. Performance comparison for various i_{an} for $D_{CO} = 6.5 \times 10^{-6}$ m^2 s^{-1}, $k_c = 4.016 \times 10^8 \exp(-29790/T)$ m s^{-1}.
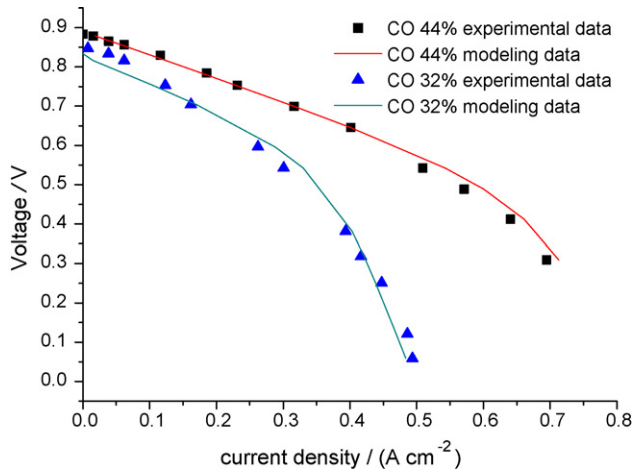
of CO:CO$_2$ = 44:56. S_{TPB} was held constant, while D_{CO} was changed for the various CO concentrations. The cell performances at 800 °C predicted by the model for CO:CO$_2$ = 44:56 and CO:CO$_2$ = 32:68 are compared with experiments in Fig. 6. The calculated polarization curves both agree very well with the experimental data. All the parameters validated by the first model were then kept the same in the second model.

The performances of SOFC with and without the carbon layer (the first and second models) are compared in Fig. 7. The results indicate that the SOFC performances of both models are very similar, with only slightly better prediction by the second model. This can be attributed to the instant consumption of CO$_2$ and the enhancement of the CO concentration in the anode, which are intrinsic features of the deposited carbon fuel cell.

The detailed influences of i_{an}, D_{CO} and k_c were than analyzed. i_{an} reflects the effect of the direct carbon electrochemical reactions. $i_{an} = 7.3 \times 10^3$ A m^{-2} was chosen as the base case for the CO SOFC. Deposited carbon fuel cells may have a higher i_{an} than CO SOFCs because it is reported that the surface carbon is a more active reducer than hydrogen [20]. Thus, a 10-times larger value of $i_{an} = 7.3 \times 10^4$ A m^{-2}, which is in the range of that for a hydrogen SOFC [14], was used for comparison. In addition, a smaller value of 7.3×10^2 A m^{-2} was also used in case the deposited carbon might react slowly. The performances for the various i_{an} are compared in Fig. 8. At the highest value, which is the highest rate among all kinds
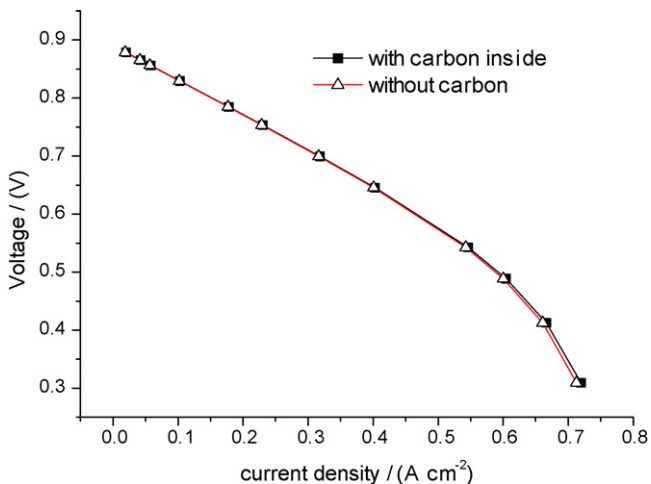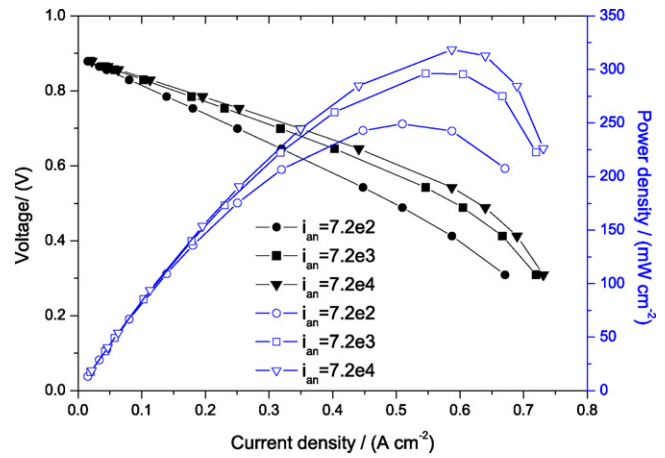
of fuels cells, the maximum power density increased only 7.5%. At the lowest value of 7.3×10^2 A m^{-2}, the power density was reduced by only 15.9%. Thus, even if the anodic electrochemical reactions were enhanced by direct electrochemical carbon reaction, the performance increase would not be very large. However, if the anodic electrochemical reactions were reduced due to solid–solid reactions rather than gas–solid reactions, the performance reduction would be more obvious.

In these calculations, D_{CO} was kept the same as in the first model. However, when carbon is deposited in the anode, D_{CO} can vary. Generally, free molecular and Knudsen diffusion are believed to occur together in the SOFC anode with the CO diffusion coefficient D_{CO} given by $D_{CO} = (\varepsilon/\tau) \cdot (1/D_{K,CO} + 1/D_{CO,CO_2})$ where ε is the anode porosity (in volume fraction) and τ is the tortuosity factor [13] which depends on the geometry and the local fluid flows [21]. Deposited carbon in the anode can greatly reduce the porosity and increase the tortuosity of the anode according to the results in Table 2. To have an estimation of the deposited carbon's influence on interior diffusion in different feeding conditions, the porosities in Table 2 in the working conditions of 50% methane feeding for 10 min and 50% methane for 30 min are used for comparison. τ is then calculated from the figure in [22] describing the relation of porosity and tortuosity. Thus, D_{CO} equals to 3.3×10^{-6} m^2 s^{-1} with 50% methane feeding for 10 min and equals to 9.9×10^{-7} m^2 s^{-1} with 50% methane feeding for 30 min. The comparison of the two cases as well as the base case is shown in Fig. 9.

Fig. 9 illustrates that the maximum power densities are reduced by 32.6% with 50% methane feeding for 10 min and reduced by 67.8% with 50% methane feeding for 30 min. The results suggest that deposited carbon will harm the interior diffusion obviously. Different length of time and different methane concentrations can cause quite different situations inside the anode, and that long flow times can seriously clog the micropores. Thus, a proper choice of deposition conditions is crucial to improve the performances of deposited carbon SOFC. Moreover, compared to the predictions in Fig. 8, D_{CO} is much more important than i_{an}.

Different deposition temperatures create different types of deposited carbons with different reactivities. As seen from Fig. 10, when the kinetic rate constant k_c (equals to $k_c = 4.016 \times 10^8 \exp(-29790/T)$ m s^{-1} [15]) is arbitrarily increased 10- and 100-fold, the maximum power densities are enhanced 6% and 40%, respectively. So if the gasification reactivity of the deposited carbons can be greatly improved, the performance will be significantly enhanced. The gasification reactivity of deposited carbon is dependent on both S_c and k_c, so different deposition
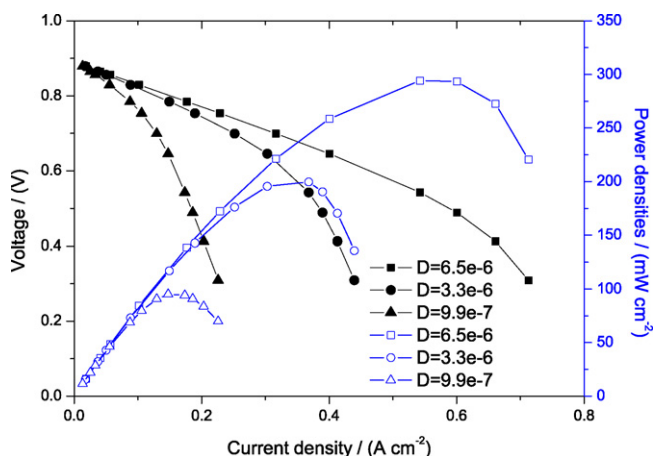

Fig. 7. Performance comparison with and without carbon.

Fig. 9. Performances comparison for various D_{CO} for $i_{an} = 7.3 \times 10^3\,\mathrm{A\,m^{-2}}$, $k_c = 4.016 \times 10^8 \exp(-29790/T)\,\mathrm{m\,s^{-1}}$.

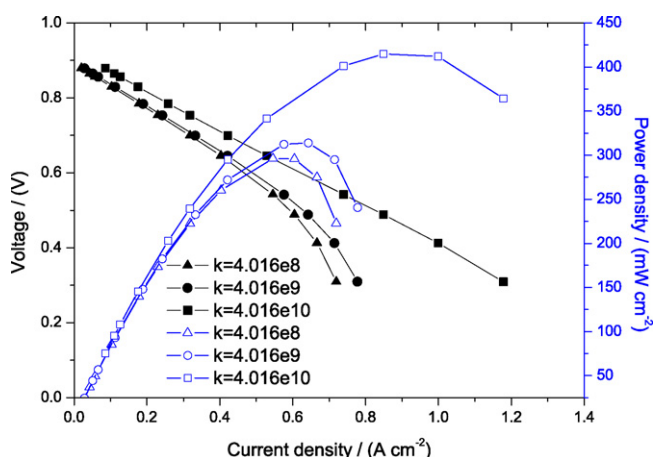**Fig. 10.** Performances comparison for various k_c for $D_{CO} = 6.5 \times 10^{-6}\,\mathrm{m^2\,s^{-1}}$, $i_{an} = 7.3 \times 10^3\,\mathrm{A\,m^{-2}}$.

conditions will result in different reactivities [23]. However, enhancement of the carbons gasification reactivity will request careful selection of the deposition temperature.

Comparison of Figs. 8–10 show that the cell performance has similar sensitivities to i_{an} and k_c and is more sensitive to D_{CO}. k_c can be more easily increased 10-fold or even more by carefully selecting the deposition conditions, while i_{an} is difficult to increase. The influence of D_{CO} is expected to be much more than k_c or i_{an}. Therefore, more attention should be paid to improving the diffusion inside the anode, rather than enlarging the electrochemical reaction sites of the deposited carbon.

5. Conclusions

Experimental and theoretical analyses were conducted to evaluate the influences of the electrochemical reactions, carbon gasification reactions and interior diffusion on the performance of deposited carbon fuel cells. The results show that:

(1) The carbon deposition experiments using Ni and YSZ powders showed a weight increase of 1% with the Ni powder as bed material, with no appreciable increase observed with the YSZ powder. Thus, the carbon tends to deposit on the Ni surface.
(2) Measurements of the carbon deposition on small chips of used cells showed that the deposited carbon distribution was not uniform through the anode thickness with little carbon deposited in the intense electrochemical reactions zones. Moreover, the primary deposited carbon particles ranged in size from 1 to 10 μm, comparable to the sizes of the anodic YSZ and Ni particles. Thus, the deposited carbon is expected to have little opportunity to directly participate in the electrochemical reactions.
(3) Modeling of the influences of the electrochemical reactions, carbon gasification reactions and interior diffusion showed that D_{CO} has a much stronger influence on the fuel cell performance than k_c or i_{an}.
(4) Both the experimental and theoretical results indicate that higher methane concentrations and shorter deposition times should be used to "charge" carbon into the anode so as not to reduce the diffusion by over-sintering of the carbon. Proper operating conditions such as the decomposition time, concentration and temperature could lead to an efficient utilize hydrocarbons in deposited carbon fuel cells.

Acknowledgments

References

[1] B. Heydorn, S. Crounch-Baker, Fuel Cell Rev. 2 (2006) 15–22.
[2] S. Li, A.C. Lee, R.E. Mitchell, T.M. Gür, Solid State Ionics 179 (2008) 1549–1552.
[3] J.F. Cooper, Fuel Cell Science, Engineering and Technology, 2004, p. 375.
[4] S. Zecevic, E.M. Patton, P. Parhami, Fuel Cell Science, Engineering and Technology, 2005, p. 507.
[5] N. Nakagawa, M. Ishida, Ind. Eng. Chem. Res. 27 (1988) 1181–1185.
[6] T.M. Gür, R.A. Huggins, J. Electrochem. Soc. 139 (1992) L95–L97.
[7] M. Ihara, S. Hasegawa, J. Electrochem. Soc. 153 (2006) A1544–A1546.
[8] M. Ihara, K. Matsuda, H. Sato, C. Yokoyama, Solid State Ionics 175 (2004) 51–54.
[9] T. Huang, M. Huang, J. Power Sources 168 (2007) 229–235.
[10] T. Huang, M. Huang, Chem. Eng. J. 135 (2008) 216–223.
[11] S. Belelis, C.G. Vayenas, J. Catal. 118 (1989) 125–146.
[12] T. Horita, N. Sakai, T. Kawada, H. Yokokawa, M. Dokiya, US Patent No. 6183896 B1 (2001).
[13] Y. Jiang, A.V. Virkar, J. Electrochem. Soc. 150 (2003) A942–A951.
[14] Y. Shi, N. Cai, C. Li, J. Power Sources 164 (2007) 639–648.
[15] S.R. Turns, An Introduction to Combustion: Concepts and Applications, second Ed., McGraw-Hill, 2000, p. 539.
[16] V.R. Choudhary, S. Banerjee, A.M. Rajput, Appl. Catal. A: Gen. 234 (2002) 259–270.
[17] Y. Lin, Z. Zhan, J. Liu, S.A. Barnett, Solid State Ionics 176 (2005) 1827–1835.
[18] Y. Shi, N. Cai, C. Li, C. Bao, E. Croiset, J. Qian, Q. Hu, S. Wang, J. Power Sources 172 (2007) 235–245.
[19] C.H. Bartholomew, Appl. Catal. A: Gen. 212 (2001) 17–60.
[20] R.T. Baker, I.S. Metcalfe, Ind. Eng. Chem. Res. 34 (1995) 1558.
[21] P. Asinari, M.C. Quaglia, M.R. von Spakovsky, B.V. Kasula, J. Power Sources 170 (2007) 359–375.
[22] J.M. Zalc, S. Reyes, E. Iglesia, Chem. Eng. Sci. 59 (2004) 2947–2960.
[23] H. He, J.M. Hill, Appl. Catal. A: Gen. 317 (2007) 284–292.